JOURNAL OF COMPUTATIONAL PHYSICS **128,** 165–180 (1996)
ARTICLE NO. 0201

A Legendre Pseudospectral Viscosity Method

S. M. OULD KABER*

Laboratoire d'Analyse Numérique, Université Pierre et Marie Curie, Paris, France and A.S.C.I., Orsay, France

Received August 3, 1995; revised April 29, 1996

We use the Legendre spectral viscosity method to solve nonlinear conservation laws. This method essentially consists in adding a spectral viscosity to the equations for the high wavenumbers of the numerical solution. This viscosity is sufficient to stabilize the numerical scheme while small enough to retain spectral accuracy. Several tests are considered including the 1D and 2D Euler equations of gas dynamics. © 1996 Academic Press, Inc.

1. INTRODUCTION

Consider the following problem, find $u(x, t)$ solution of the scalar conservation law

$$\partial_t u + \partial_x f(u) = 0 \tag{1.1}$$

associated with the initial data

$$u(x, 0) = u_0(x) \tag{1.2}$$

and appropriate boundary conditions. Here $t > 0$, x lies in some open interval Ω of $\mathbb{R}$ and the flux f is a regular function of u. It is well known that solutions of Eq. (1.1) may develop discontinuities even if the initial data u_0 is regular. Hence there may be no classical (i.e., smooth) solution of this equation after certain critical time t_s. To overcome this, one defines weak solutions [12], as solutions satisfying, for all test function $\varphi \in \mathscr{C}_0^\infty(\Omega \times \mathbb{R}^+)$

$$\iint_{\Omega\times\mathbb{R}^+} (u\partial_t\varphi + f(u)\partial_x\varphi)\, dx\, dt + \int_\Omega u_0\varphi\, dx = 0. \tag{1.3}$$

Such weak solutions may not be unique; in order to ensure the uniqueness of the solution, and for physical reasons one imposes that the weak solution satisfies an additional inequality called entropy inequality,

$$\partial_t U(u) + \partial_x F(u) \le 0, \tag{1.4}$$

where the entropy function U is a regular function and the entropy flux F is related to U and to the flux f by $F' = U'f'$. The (weak) solution of (1.1)–(1.4) is then unique.

In this paper, we are interested in computing the *entropic solution* of Eq. (1.1), i.e., the unique weak solution satisfying the entropy inequality (1.4) for all convex entropy U. This will be obtained by using spectral methods.

Spectral methods consist in finding the first Fourier-like coefficients of the solution of partial differential equations (pure spectral method) or the values of this solution at some Gauss nodes (collocation method). These methods have been used successfully in the computation of regular solutions of PDE [3, 5]. The rate of covergence of the numerical solution u^N depends on the regularity of the exact solution u; for example, if u is $\mathscr{C}^\infty$-regular then the error $\|u - u^N\|$ goes to 0 faster than any power of $1/N$; this is the so-called *spectral accuracy*.

This attractive accuracy property is desirable when applying spectral methods to hyperbolic laws. Unfortunately, the solutions of such problems may develop discontinuities and it is well known that polynomial approximations of discontinuous functions exhibit spurious oscillations (Gibbs phenomenon) that slow down their convergence. Let (φ_k) denote either the Fourier or Legendre basis, $u(x, t) = \sum_k \hat{u}_k(t)\varphi_k(x)$ the solution of the considered problem and $u^N(x, t) = \sum_{|k|\le N} \hat{u}_k^N(t)\varphi_k(x)$ the numerical solution obtained by a spectral method. Since the truncated series $\pi_N u(x, t) = \sum_{|k|\le N} \hat{u}_k(t)\varphi_k(x)$ is the best approximation of u (in the L^2 sense) by polynomials of degree $\le N$, the error $\|u^N - u\|$ is larger than $\|\pi_N u - u\|$ which decreases at most like $1/N$ when the solution u contains discontinuities. This slow convergence is inherent to the Gibbs phenomenon.

It is clear that one must pay attention when applying spectral methods to solve problems with discontinuous solutions; the oscillations produced by the Gibbs phenomenon often grow up due to the nonlinearities and the calculations fail. A key issue is the control of the Gibbs phenomenon, this is obtained by the Legendre spectral vanishing viscosity (LSVV) method which is presented in this paper. This method consists in adding a small viscosity on the high coefficients of the numerical solution. This viscosity is shown to be at the same time small enough to retain the spectral accuracy and strong enough to stabilize the computations so that it ensures the convergence to

* E-mail: ould@ann.jussieu.fr.

0021-9991/96 $18.00

the entropic solution. The polynomial approximation u^N is defined as the unique solution of the variational problem (2.6). It can also be viewed as the solution of two collocation problems: one is defined in the interior of the domain; the other is defined at the boundaries of the domain (see Eq. (3.1)–(3.2)).

Note that, unlike most of the spectral schemes for hyperbolic equations, the SVV method is a *shock capturing* method; hence it does not require the computation of the location of the discontinuities.

Recently, a Chebyshev spectral viscosity method (CSVV) was successfully applied in [2] for the simulation of waves in a stratified atmosphere.

The main difference between the Chebyshev and the Legendre spectral vanishing viscosity method relies on the choice of collocation points. The interest of the Chebyshev method is related to the possibility of using a fast transform to compute the nonlinear products. This feature is noticeable when using polynomials of degree larger than 100 (say). This is the case for problems with complicated structures for which high order of approximation is required.

The interest of the Legendre approximation, on the other hand, relies on the relative ease for handling the boundary conditions (see the literature on the spectral element method for elliptic problems); instead of using a very high degree polynomial the idea is based on breaking up the domain into smaller pieces and approximating the solution by piecewise polynomials of degree less than 100. We refer to [8] for more details on this approach. On the theoretical side, the analysis of the Legendre spectral approximation is easier than for the Chebyshev approximation since this latter method requires weighted spaces; consult [3].

We will compute also the solutions of systems of conservation laws. The problem is to find $\mathbf{u}(x, t) = (u_1, ..., u_p) \in \mathbb{R}^p$ such that

$$\partial_t \mathbf{u} + \partial_x \mathbf{f}(\mathbf{u}) = 0 \tag{1.5}$$

and $\mathbf{u}(x, 0) = \mathbf{u}_0(x)$, where $\mathbf{f}$: $\mathbb{R}^p \to \mathbb{R}^p$ is a vector function.

We are interested also in computing the solutions of multidimensional systems which involve different fluxes; for example, in the 2D case the problem is to find $\mathbf{u}(x, y, t) = (u_1, ..., u_p) \in \mathbb{R}^p$ satisfying

$$\partial_t \mathbf{u} + \partial_x \mathbf{f}(\mathbf{u}) + \partial_y \mathbf{g}(\mathbf{u}) = 0 \tag{1.6}$$

and the initial condition $\mathbf{u}(x, y, 0) = \mathbf{u}_0(x, y)$.

The organization of the paper is as follows: in Section 2 we introduce the Legendre spectral viscosity method. In Section 3, we show how to implement this method. In Section 4 we solve some test problems that prove its efficiency. Finally Section 5 is devoted to some concluding remarks.

2. THE LEGENDRE VISCOSITY METHOD

We first present the original spectral (Fourier) viscosity method or spectral vanishing viscosity (SVV) method introduced in [19]. Consider Eq. (1.1) with 2π-periodic boundary conditions; the solution is then 2π-periodic,

$$u(x, t) = \sum_{k=-\infty}^{+\infty} \hat{u}_k(t) e^{ikx}. \tag{2.1}$$

The spectral (Fourier) approximation of Eq. (1.1) leads to finding $u^N(x, t)$ such that

$$\partial_t u^N + \partial_x \pi_N f(u^N) = 0 \tag{2.2}$$

$$u^N(x, 0) = \pi_N u_0(x), \tag{2.3}$$

where u^N belong to the space $\mathbb{S}_N$ of trigonometric polynomials of degree less than or equal to N and π_N is the L^2-orthogonal projection onto $\mathbb{S}_N$. It can be shown [20] that, unless the flux f is genuinely nonlinear (i.e., $f'' \equiv 0$), u^N cannot converge even weakly to the entropic solution u. However, (2.2) is a spectrally accurate approximation of the conservation law (1.1) since the discretisation error (in a weak norm) is

$$\|(\mathcal{I} - \pi_N) f(u^N)\|_{H^{-s}} \le C N^{-s} \|u\|_{L^2} \quad \forall s \ge 0. \tag{2.4}$$

In order to overcome the lack of convergence of the scheme while retaining the infinite high order accuracy (2.4), Tadmor [19] proposed adding artificial viscosity on the high Fourier modes of (2.2), the problem is then to find $u^N(x, t) \in \mathbb{S}_N$ such that

$$\partial_t u^N + \partial_x \pi_N f(u^N) = \varepsilon \partial_x \mathcal{Q}_m \partial_x u^N, \tag{2.5}$$

where

- $\varepsilon = \varepsilon_N$ is the (positive) viscosity amplitude, recall that without viscosity (i.e., $\varepsilon_N = 0$) the spectral solution does not converge to the entropic solution, actually ε_N must not decrease too fast to 0 (at most as $1/N$).
- $\mathcal{Q}_m$ denotes the spectral viscosity operator defined for $v = \sum_{k=-\infty}^{+\infty} \hat{v}_k e^{ikx}$ by $\mathcal{Q}_m v = \sum_{k=-N}^{N} \hat{q}_k \hat{v}_k e^{ikx}$; the viscosity coefficients satisfy

$$\hat{q}_k = 0 \quad \text{for } |k| \le m_N, \quad 0 \le \hat{q}_k \le 1 \quad \text{for } m_N < |k| \le N.$$

The viscosity operator $\mathcal{Q}_m$ acts only on the high wavenumbers, the parameter m_N indicates the level from which this operator acts, it is supposed that

$$\lim_{N \to +\infty} m_N = +\infty.$$

This scheme is analysed in [13], where the L_∞ boundedness and the convergence, via compensated compactness arguments, are proven: at any time $T > 0$,

$$u^N(\cdot, T) \to u(\cdot, T) \quad \text{strong in } L^2.$$

This is a slow convergence since the best polynomial approximation (in the L^2 sense) of

$$u(x, T) = \sum_{k=-\infty}^{+\infty} \hat{u}_k(T) e^{ikx}$$

is given by the truncated series

$$\pi_N u(x, T) = \sum_{k=-N}^{N} \hat{u}_k(T) e^{ikx}$$

and when u is discontinuous, the error $\|\pi_N u - u\|$ decreases like $\mathcal{O}(1/N)$; hence the convergence rate of $u^N(\cdot, T)$ is at most 1. Actually the following convergence rate of the spectral viscosity solution (take $m = N^\beta$) is proven in [18]:

$$\|u^N(\cdot, T) - u(\cdot, T)\|_{L^1} \le CN^{-\beta}, \quad \beta < \tfrac{1}{2}.$$

The scheme (2.5) may be interpreted as a way to add a small viscosity on the high wavenumbers. To see that consider the system of ordinary differential equations satisfied by the Fourier coefficients of the numerical solution $u^N(x, t) = \sum_{k=-N}^{N} \hat{u}_k^N(t) e^{ikx}$,

$$\frac{d}{dt}\hat{u}_k^N(t) + \widehat{f(u^N)}_k = 0 \qquad \text{for } |k| \le m_N,$$

$$\frac{d}{dt}\hat{u}_k^N(t) + \widehat{f(u^N)}_k = -\varepsilon_N k^2 \hat{q}_k \hat{u}_k^N(t) \quad \text{for } m_N < |k| \le N.$$

The evolution of the inviscid portion of the spectrum ($|k| \le m_N$) follows the original conservation law (1.1), while the last portion of the spectrum ($m_N < |k| \le N$) is damped.

When the approximated solution u is not periodic, the LSVV method introduced in [14] is defined by finding $u^N(x, t)$ in the space $\mathbb{P}_N$ of algebraic polynomials of degree less than or equal to N as the solution of the following variational problem: for all φ in $\mathbb{P}_N$

$$\begin{aligned}(\partial_t u^N + \partial_x \mathcal{I}_N f(u^N), \varphi)_N \\ = -\varepsilon_N (\mathcal{Q}_m \partial_x u^N, \partial_x \varphi)_N + (\mathcal{B}(u^N), \varphi)_N,\end{aligned} \tag{2.6}$$

where

- $u^N = \sum_{k=0}^{N} \hat{u}_k^N L_k$ is the numerical solution spanned in the Legendre basis $(L_k)_{k\ge 0}$. The Legendre polynomials are defined by $L_0(x) = 1$, $L_1(x) = x$, and the recurrence formula $(n+1)L_{n+1}(x) = (2n+1)xL_n(x) - nL_{n-1}(x)$. They are orthogonal on $[-1, 1]$ for the usual scalar product,

$$\int_{-1}^{1} L_n(x) L_m(x)\, dx = \frac{2}{2n+1}\delta_{n,m}$$

($\delta_{n,m}$ is the Kronecker symbol).

- $\mathcal{Q}_m$ denotes now the Legendre viscosity operator defined for $v = \sum_{k=0}^{+\infty} \hat{v}_k L_k$ by $\mathcal{Q}_m v = \sum_{k=0}^{N} \hat{q}_k \hat{v}_k L_k$.

- $\mathcal{B}(u^N)$ is a polynomial of degree less or equal than N which should enable $u^N(x, t)$ to satisfy exactly the required inflow boundary conditions.

- $\mathcal{I}_N$ is the interpolation operator at the Gauss–Lobatto Legendre quadrature points and $(\cdot, \cdot)_N$ is the associated discrete scalar product. For continuous functions u and v,

$$(u, v)_N = \sum_{i=0}^{N} u(\xi_i) v(\xi_i) w_i,$$

where the ξ_i's and the w_i's are respectively the nodes and weights of the Gauss-Lobatto Legendre quadrature formula:

$$\int_{-1}^{1} v(x)\, dx \simeq \sum_{i=0}^{N} v(\xi_i) w_i, \tag{2.7}$$

this formula being exact for $v \in \mathbb{P}_{2N-1}$.

For the analysis of the scheme (2.6), we refer to [14] where the convergence of u^N toward the entropic solution is proven assuming $1 - (m_N/k)^4 \le \hat{q}_k \le 1$ for $k > m_N$.

We present now the algorithm for computing the spectral approximation of a nonlinear conservation law; there are two different steps, namely:

- Applying the spectral viscosity method to *stabilize* the scheme, this step gives a polynomial u^N. When the exact solution u contains discontinuities, this approximation is oscillatory and at most first order.

- To recover a spectral accuracy, u^N is posttreated (at the end of the computation) by filtering; this step will be described in the next section.

3. IMPLEMENTATION

3.1. *1D Scalar*

First observe that the Legendre viscosity method (2.6) can be implemented as a collocation method. For the sake of simplicity, let us consider the case where there is an inflow condition at $x = -1$ and an outflow condition at $x = +1$, in this case the polynomial $\mathcal{B}(u_N)$ is

$$\mathscr{B}(u^N)(\xi,t) = \tau(t)(1-\xi)L'_N(\xi),$$

so it vanishes at all the collocation points except the inflow boundary -1 (recall that the Legendre Gauss Lobatto points are the $N+1$ zeros of $(1-x^2)L'_N(x)$). The parameter $\tau(t)$ allows for imposing exactly the boundary conditions and is not computed.

Now take $\varphi = h_i$ in (2.6), where h_i is the Lagrange characteristic polynomial of $\mathbb{P}_N$ associated with the nodes ξ_i, satisfying $h_i(\xi_j) = \delta_{ij}$, $0 \le i, j \le N$. Straightforward computations give (use summation by parts and exactness of formula (2.7) for $v \in \mathbb{P}_{2N-1}$):

• At the interior nodes $1 \le i \le N-1$,

$$\partial_t u^N(\xi_i,t) + \partial_x \mathscr{I}_N f(u^N)(\xi_i,t) = \varepsilon_N \partial_x \mathscr{Q}_m(\partial_x u^N)(\xi_i,t), \tag{3.1}$$

this is Eq. (2.6), regularized by a viscous term and discretized by a standard collocation method.

• At the outflow boundary $x = 1$:

$$\begin{aligned}\partial_t u^N(+1,t) + \partial_x \mathscr{I}_N f(u^N)(+1,t) \\ = \varepsilon_N \partial_x \mathscr{Q}_m(\partial_x u^N)(+1,t) - \frac{\varepsilon_N}{\omega_N}\mathscr{Q}_m(\partial_x u^N)(+1,t).\end{aligned} \tag{3.2}$$

The strange term on the right-hand side of (3.2) prevents the creation of a boundary layer. Equations (3.1)–(3.2), together with the prescribed inflow data $u^N(-1,t) = g(t)$, give an easy implementation of the viscosity approximation (2.6).

For an efficient resolution of (3.1), we construct two linear operators:

• The Legendre differentiation operator $\mathscr{D}_N$. Given the $(N+1)$ values $v(\xi_i)$ of a function v at the collocation points ξ_i, we define the $(N+1)\times(N+1)$ matrix $\mathscr{D}_N$ by

$$\mathscr{D}_N \begin{pmatrix} v(\xi_0) \\ \vdots \\ v(\xi_N) \end{pmatrix} = \begin{pmatrix} \partial_x(\mathscr{I}_N v)(\xi_0) \\ \vdots \\ \partial_x(\mathscr{I}_N v)(\xi_N) \end{pmatrix}.$$

Writing

$$\mathscr{I}_N u(x) = \sum_{i=0}^{N} u_i h_i(x),$$

it follows that

$$\partial_x(\mathscr{I}_N u)(x) = \sum_{i=0}^{N} u_i \partial_x h_i(x),$$

and then the coefficients of $\mathscr{D}_N$ are

$$\mathscr{D}_N(i,j) = h'_j(\xi_i), \quad 0 \le i, j \le N.$$

• The Legendre viscosity operator $\mathscr{V}_m$. Given the $(N+1)$ values $v(\xi_i)$ of a function v at the collocation points ξ_i, we define the $(N+1)\times(N+1)$ matrix $\mathscr{V}_m$ by

$$\mathscr{V}_m \begin{pmatrix} v(\xi_0) \\ \vdots \\ v(\xi_N) \end{pmatrix} = \begin{pmatrix} \partial_x \mathscr{Q}_m \partial_x(\mathscr{I}_N v)(\xi_0) \\ \vdots \\ \partial_x \mathscr{Q}_m \partial_x(\mathscr{I}_N v)(\xi_N) \end{pmatrix}.$$

Clearly,

$$\partial_x \mathscr{Q}_m \partial_x(\mathscr{I}_N v)(x) = \sum_{i=0}^{N} u_i \partial_x \mathscr{Q}_m \partial_x(h_i)(x),$$

and the coefficients of $\mathscr{V}_m$ are

$$\mathscr{V}_m(i,j) = \partial_x \mathscr{Q}_m \partial_x(h_j)(\xi_i), \quad 0 \le i, j \le N.$$

Equation (3.1) can now be written in a compact form

$$\frac{d}{dt} U_N + \mathscr{D}_N F_N = \varepsilon_N \mathscr{V}_m U_N, \tag{3.3}$$

where

$$U_N = \begin{pmatrix} u^N(\xi_0) \\ \vdots \\ u^N(\xi_N) \end{pmatrix}, \quad F_N = \begin{pmatrix} f(u^N)(\xi_0) \\ \vdots \\ f(u^N)(\xi_N) \end{pmatrix}.$$

Remark. Equation (3.3) is modified at the boundaries to take into account the boundary conditions; for example, if $x = 1$ is an outflow boundary, the extra term in the right-hand side of (3.2) is added to the last line of (3.3).

We discretise the differential equation (3.3) as follows: let δt denote the time step and U_N^n the approximation at time $t_n = n\delta t$. An Adams–Bashforth-type scheme of order 2 leads to

$$\frac{U_N^{n+1} - U_N^n}{\delta t} + \mathscr{D}_N F_N^{n+1/2} = \varepsilon_N \mathscr{V}_m U_N^n,$$

where $F_N^{n+1/2}$ is a conservative extrapolation of F_N at time $t_{n+1/2} = t_n + \delta t/2$:

$$F_N^{n+1/2} = F_N(U^{N,n+1/2}), \quad U^{N,n+1/2} = \tfrac{3}{2}U^{N,n} - \tfrac{1}{2}U^{N,n-1}. \quad (3.4)$$

The restriction on the time step δt is determined by the usual CFL-like condition for spectral methods (see [10]),

$$\delta t \le C\frac{1}{N^2},$$

according to the concentration of the Gauss points near ± 1.

Remark. The implementation of the LSVV method does not require the usual (but expensive) reconstruction from cell averages to point values.

3.2. *1D Systems*

We will show in the next section the efficiency of the LSVV method for scalar problems. A natural way to extend it for systems consists in turning the system from the conservative form into the characteristic one. The viscosity is then applied on the characteristic variables. However, as well known the computation of the solutions of nonlinear conservation laws requires the use of the conservative form of these equations; otherwise, the calculations give a false (nonentropic) solution. The transformation from the conservative form to the characteristic one and vice versa must be done at every time step. This switch back and forth is very time consuming but sometimes necessary. Consult the finite differences literature about this. Here we apply the viscosity *directly* on the conservative variables; the fluxes are evaluated *pointwisely* and this provides good results. Let us notice that the LSVV method for system does not require neither cell averaging technique, nor field by field decomposition.

At the interior nodes, the LSVV approximation of system (1.5) is

$$\partial_t \mathbf{u}^N(\xi_i, t) + \partial_x \mathcal{I}_N \mathbf{f}(\mathbf{u}^N)(\xi_i, t) = \mathcal{Q}(\mathbf{u}^N). \quad (3.5)$$

Here, $\mathbf{u}^N \equiv (u_1^N, ..., u_p^N)^{\mathrm{T}} \in \mathbb{P}_N^p$ denotes the polynomial approximation of the vector $\mathbf{u} = (u_1, ..., u_p)^{\mathrm{T}}$, and $\mathcal{Q}$ is a general $p \times p$ spectral viscosity matrix which is activated only on high Legendre modes. Using obvious notations, the system (3.5) is written as

$$\frac{d}{dt}\begin{pmatrix} U_{N,1} \\ \vdots \\ U_{N,p} \end{pmatrix} + \begin{pmatrix} \mathcal{D}_N & 0 & 0 \\ \vdots & \ddots & \vdots \\ 0 & 0 & \mathcal{D}_N \end{pmatrix}\begin{pmatrix} F_{N,1} \\ \vdots \\ F_{N,p} \end{pmatrix} = \begin{pmatrix} \varepsilon_1 \mathcal{V}_{m1} & 0 & 0 \\ \vdots & \ddots & \vdots \\ 0 & 0 & \varepsilon_p \mathcal{V}_{mp} \end{pmatrix}\begin{pmatrix} U_{N,1} \\ \vdots \\ U_{N,p} \end{pmatrix}. \quad (3.6)$$

3.3. *2D Systems*

For the two-dimensional system (1.6), the right-hand side of (3.6) must be replaced by (for the sake of clearness we consider the case where the number of nodes is the same in each direction)

$$\sum_{i=1}^{4}\begin{pmatrix} \varepsilon_1^i \mathcal{V}_{m_1^i} & 0 & 0 \\ \vdots & \ddots & \vdots \\ 0 & 0 & \varepsilon_p^i \mathcal{V}_{m_p^i} \end{pmatrix}\begin{pmatrix} U_{N,1} \\ \vdots \\ U_{N,p} \end{pmatrix}, \quad (3.7)$$

where

$$\mathcal{V}_{m_k^1} = \partial_x \mathcal{Q}_{m_k^1} \partial_x, \quad \mathcal{V}_{m_k^2} = \partial_x \mathcal{Q}_{m_k^2} \partial_y,$$
$$\mathcal{V}_{m_k^3} = \partial_y \mathcal{Q}_{m_k^3} \partial_x, \quad \mathcal{V}_{m_k^4} = \partial_y \mathcal{Q}_{m_k^4} \partial_y.$$

For scalar multidimensional problems this reduces to

$$\sum_{i=1}^{4} \varepsilon^i \mathcal{V}_{m^i} U_N. \quad (3.8)$$

Let us now introduce the filter used to improve the accuracy of the spectral solution in order to get a *high order* approximation.

3.4. *Filtering*

This point is motivated by the fact that informations about the exact solution are contained in this high resolution scheme

• *Spectral accuracy.* It has been proven in [1] for linear periodic hyperbolic problems that the solution u_N given by spectral (Fourier) methods at time t are very close to $\pi_N u(x, t) = \sum_{k=-N}^{N} \hat{u}_k(t) e^{ikx}$. Hence the spectral solution $u^N(\cdot, t)$ should be considered as an accurate approximation of $\pi_N u(\cdot, t)$, rather than $u(\cdot, t)$ itself in both cases of Legendre and Fourier approximations. This fact is checked numerically for nonlinear problems.

• *Physical accuracy.* It is well known that truncated series $\pi_N u$ provides highly accurate approximation of u when u is sufficiently smooth. If u is discontinuous, $\pi_N u$ produces spurious oscillations (Gibb's phenomenon) and its accuracy is deteriorated. To enhance the convergence rate in such cases, we introduce a filter $\mathcal{F}$ such that the pointwise error $|u(x) - \mathcal{F}(\pi_N u)(x)|$ is locally spectrally small.

The filter we used depends on two parameters $(\theta, \beta) \in (0, 1)^2$ and is defined by ($p = [N^\beta]$)

$$\mathcal{F}^{\theta,p} u(x) = \int_{-1}^{1} \Psi^{\theta,p}(x; y) u(y)\, dy, \quad (3.9)$$

where

$$\Psi^{\theta,p}(x;y) = \rho\left(\frac{x-y}{\theta}\right) K_p(x;y),$$

$\rho(x) \in C_0^\infty(-1, 1)$ is a localizer satisfying $\rho(0) = 1$, and $K_p(x; y)$ is the Christoffel–Darboux kernel

$$K_p(x;y) = \sum_{j=0}^{p} \frac{L_j(x)\,L_j(y)}{\|L_j\|^2}.$$

The local error $|u(x) - \mathscr{F}^{\theta,p}(\pi_N u)(x)|$ is spectrally small, except in a neighborhood of the discontinuities; consult [17] for details. The multidimensional filter is obtained by tensorisation of (3.9).

4. NUMERICAL RESULTS

Most of the tests presented here are taken from the literature about high order methods for hyperbolic problems: essentially nonoscillatory finite differences methods [15, 11] and spectral shock-fitting methods [4].

In all the computations reported in this section, the time discretization is the explicit scheme (3.4). For systems the results were obtained using a simple viscosity matrix for each component, i.e., in (3.6) we take

$$\varepsilon_1 = \cdots = \varepsilon_p, \quad m_1 = \cdots = m_p$$

and viscosity coefficients

$$\begin{aligned} \hat{q}_k &= 0 && \text{for } |k| \le m, \\ \hat{q}_k &= e^{-(k-N)^\varepsilon/(k-m)^2} && \text{for } m < |k| \le N. \end{aligned} \tag{4.1}$$

For multidimensional problems, we apply a tensorized viscosity operator for each component; i.e., in (3.7) we put

$$\varepsilon_k^2 = \varepsilon_k^3 = 0, \quad k = 1, ..., p.$$

The mode from which the viscosity acts is $m = 5\sqrt{N}$ and the viscosity amplitude is $\varepsilon_N = 1/N$.

4.1. *Example* i. *Linear Advection Equation*

We consider Eq. (1.1) in the linear case $f(u) = u$.

First, we want to verify that the LSVV method is high order accurate even at extrema points. To do this we consider the following initial data,

$$u(x, 0) = \sin^4(\pi x), \tag{4.2}$$

with periodic boundary conditions at ± 1. The exact solution is $u(x, t) = u(x - t, 0)$ so that the local errors and the accuracy are easily computed. We take $N = 40$ and present the results after one period ($t = 2$). The solution is displayed in Fig. 1; Fig. 2 shows the pointwise error $|u^N(x) - u(x)|$, while the Fig. 3 shows the L^2 error computed on a uniform grid of 100 points.

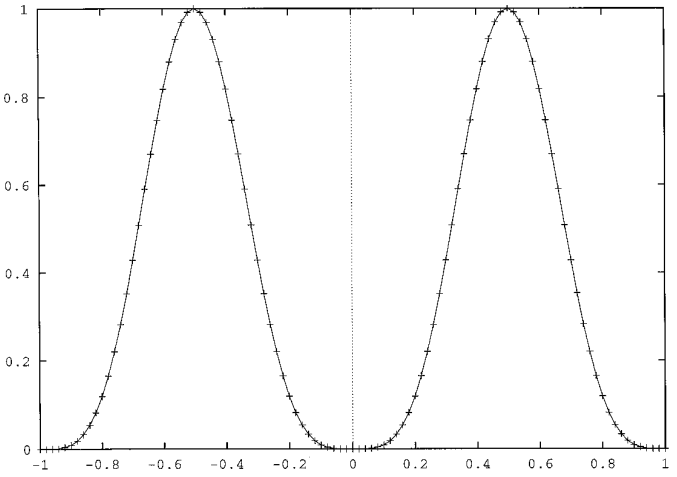

FIG. 1. Linear advection equation; exact solution (solid line) and numerical solution (+), $N = 40$, $\delta t = 5\ 10^{-3}$.

4.2. *Examples* ii. *Burgers Equation*

The inviscid Burgers equation is a model of hyperbolic scalar conservation law; it corresponds to Eq. (1.1) with quadratic flux $f(u) = \frac{1}{2}u^2$.

1. *High order accuracy.* Take the initial data:

$$u(x, 0) = -\sin(\pi x), \tag{4.3}$$

with boundary conditions $u(\pm 1, t) = 0$. The solution of

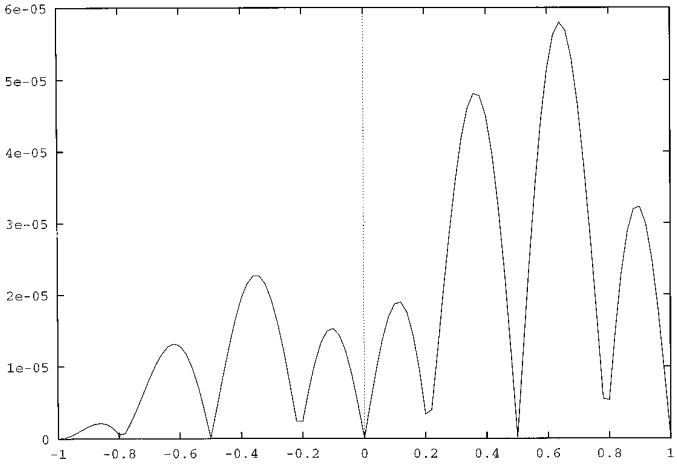

FIG. 2. Linear advection equation; the pointwise errors $|u^N(x) - u(x)|$.

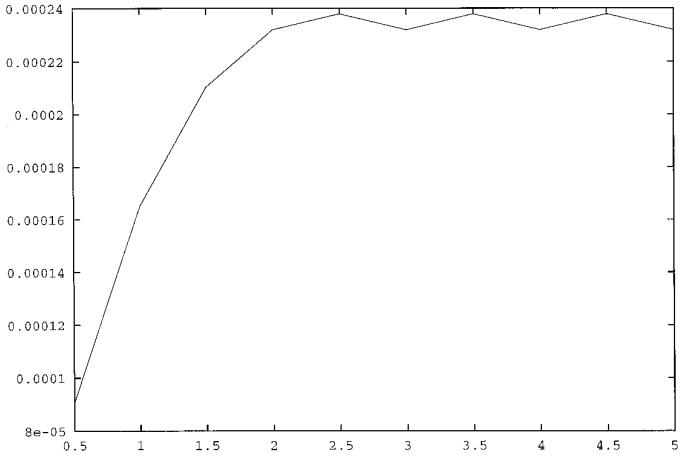

FIG. 3. Linear advection equation; error (in the L2 norm) as function of time $N = 40$.

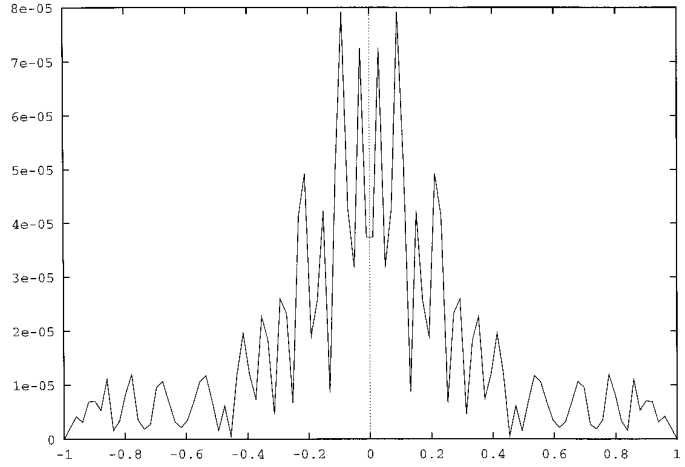

FIG. 5. Burgers equation with smooth initial data; solution at time $t = 1/2\pi$, the pointwise errors $|u^N - u|$.

this problem develops a discontinuity at time $t_s = 1/\pi$; this stationary shock is located at point $x_s = 0$. The numerical solution ($N = 49$, $\delta t = 3 \times 10^{-4}$) and the exact one for $t = t_s/2$ (before the shock was forming) are displayed Fig. 4 and the pointwise error $|u^N - u|$ is shown in Fig. 5. Clearly, the numerical solution u_N gives a high order approximation of the exact solution. However, as time t approaches the critical time t_s, the polynomial approximation u_N oscillates more and more. To get enough resolution of u (after filtering) one has to use more nodes. Figure 6 shows the oscillatory numerical approximation u^N ($N = 99$, $\delta t = 2/\pi\ 10^{-4}$) and the exact solution u, after the formation of the shock ($t = 2t_s$).

The oscillations in the polynomial u_N are not surprising since for time $t > t_s$, the solution u is discontinuous but still admits a Legendre expansion

$$u(x,t) = \sum_{k=0}^{\infty} \hat{u}_k(t) L_k(x),$$

and the best N degree polynomial approximation (for the L^2 norm) of u is given by the trucated series

$$\pi_N u(x,t) = \sum_{k=0}^{N} \hat{u}_k(t) L_k(x)$$

which is oscillatory, of course. Clearly the numerical solution $u^N(\cdot, 2t_s)$ (plotted in Fig. 6) is an oscillatory approximation of $u(\cdot, 2t_s)$ and may be considered in a first step as a bad approximation of u in the physical space (the x space). It is, however, a good approximation of u in the space of frequencies (the "Fourier" space),

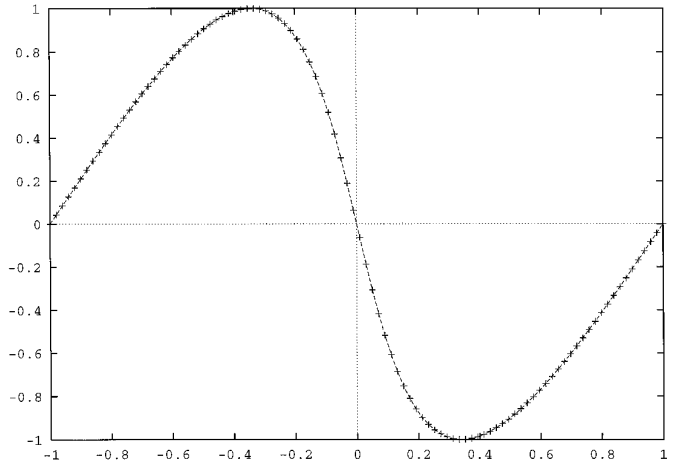

FIG. 4. Burgers equation with smooth initial data; exact solution (dashed line) and numerical solution (+) at solution at time $t = 1/2\pi$, $N = 49$, $\delta t = 3\ 10^{-4}$.

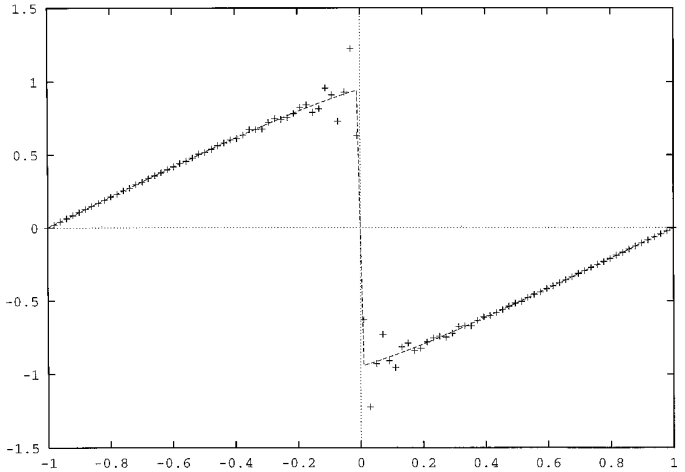

FIG. 6. Burgers equation with smooth initial data; solution at time $t = 2/\pi$, $N = 99$, $\delta t = 0.63662\ 10^{-4}$.

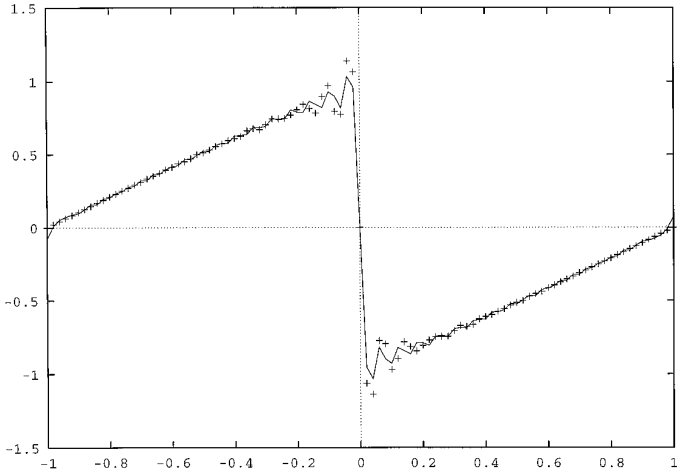

FIG. 7. Burgers equation with smooth initial data; the polynomials u^N (+) and $\pi_N u$ (solid line) at time $t = 2/\pi$.

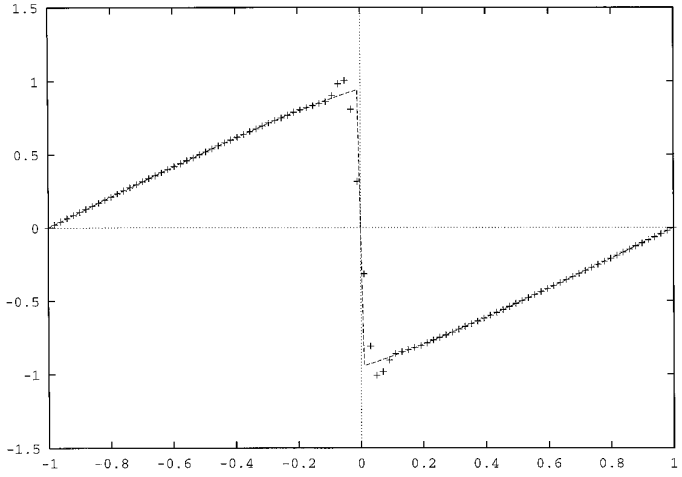

FIG. 9. Burgers equation with smooth initial data; solution at time $t = 2/\pi$; filtered solution $\mathscr{F}^{\theta,p}u^N$ with $p = 50$, $\theta = 0.3$.

to see that let us compare the two polynomials $u^N(\cdot, 2t_s)$ and $\pi_N u(\cdot, 2t_s)$ displayed in Fig. 7. For more precise comparison we plot on Fig. 8 the Legendre coefficients of the two polynomials. The coefficients $\hat{u}_k$ are computed by

$$\hat{u}_k = \frac{2k+1}{2}\left\{\int_{-1}^{0} u(x,t)L_k(x)\,dx + \int_{0}^{1} u(x,t)L_k(x)\,dx\right\},$$

where each integral is computed using a Gauss–Lobatto–Legendre formula with $M = 100$ nodes, for example,

$$\int_{-1}^{0} u(x,t)L_k(x)\,dx = \frac{1}{2}\int_{-1}^{1} u\left(\frac{y-1}{2},t\right)L_k\left(\frac{y-1}{2}\right)dy$$
$$\simeq \frac{1}{2}\sum_{i=0}^{M} u\left(\frac{\xi_i^M-1}{2},t\right)L_k\left(\frac{\xi_i^M-1}{2}\right)w_i^M.$$

Let us recall some results about the Burgers equation. For $x_0 \in \Lambda$, define in the (x, t) plane the straight lines

$$x = u_0(x_0)t + x_0; \tag{4.4}$$

the solution u is constant along such lines (called characteristics),

$$u(x,t) = u_0(x_0).$$

Hence to compute $u(x, t)$ we search for x_0 (foot of the characteristic) defined by Eq. (4.4) (or compute directly u using the implicit relation $u(x, t) = u_0(x - tu(x, t))$. Discontinuity appears when this equation has more than one solution. In our case it is very easy to select the good root corresponding to the entropic solution. The values $u(x, t)$ are evaluated with the machine precision using the bissection method to compute x_0 from (4.4).

The coefficients $\hat{u}_k(2t_s)$ and $\hat{u}_{N,k}(2t_s)$ are displayed in Fig. 8. Clearly the coefficients of the numerical solution are close (except the higher ones) to those of the exact solution. This motivates the use of the filtering procedure briefly presented in the previous section since it is proven in [16] that such a filter, when applied to $\pi_N u$ gives a highly accurate approximation of u, except near the discontinuity. Figure 9 shows the filtered numerical solution (with filter parameters $\theta = 0.3$, $p = 50$) and the exact solution. We present the pointwise errors $|u^N - u|$ and $|\mathscr{F}u^N - u|$ in

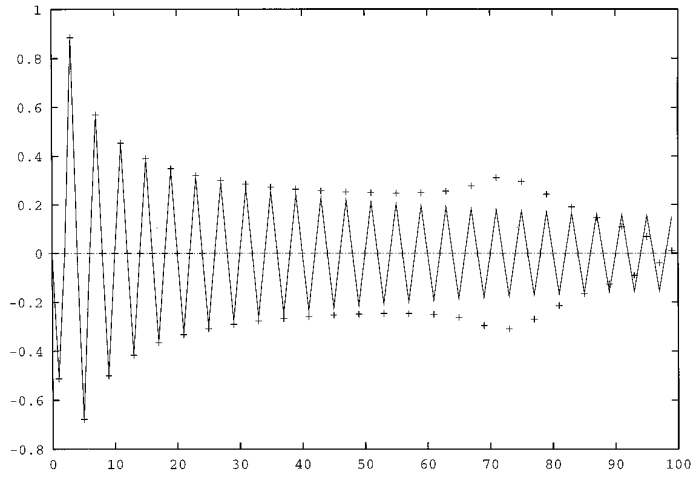

FIG. 8. Burgers equation with smooth initial data; Legendre coefficients of u^N (+) and u (solid line) at time $t = 2/\pi$.

TABLE I

Burgers Equation with Smooth Initial Data

x	$\lvert u^N(x) - u(x)\rvert$	$\lvert Fu^N(x) - u(x)\rvert$
−1.00000	0.26368 10^{-15}	0.83106 10^{-03}
−0.90000	0.23890 10^{-03}	0.21983 10^{-04}
−0.80000	0.75911 10^{-03}	0.69810 10^{-04}
−0.70000	0.18199 10^{-02}	0.19575 10^{-03}
−0.60000	0.11610 10^{-02}	0.93667 10^{-04}
−0.50000	0.14850 10^{-02}	0.15630 10^{-03}
−0.40000	0.37973 10^{-02}	0.15813 10^{-03}
−0.30000	0.23102 10^{-02}	0.10403 10^{-02}
−0.20000	0.10124 10^{-01}	0.28235 10^{-02}
−0.10000	0.91660 10^{-01}	0.96456 10^{-03}
0.00000	0.94775 10^{+00}	0.94775 10^{+00}
0.10000	0.91660 10^{-01}	0.96456 10^{-03}
0.20000	0.10124 10^{-01}	0.28235 10^{-02}
0.30000	0.23102 10^{-02}	0.10403 10^{-02}
0.40000	0.37973 10^{-02}	0.15813 10^{-03}
0.50000	0.14850 10^{-02}	0.15630 10^{-03}
0.60000	0.11610 10^{-02}	0.93667 10^{-04}
0.70000	0.18199 10^{-02}	0.19575 10^{-03}
0.80000	0.75911 10^{-03}	0.69810 10^{-04}
0.90000	0.23890 10^{-03}	0.21983 10^{-04}
1.00000	0.00000 10^{+00}	0.83106 10^{-03}

Note. Pointwise errors after the shock appears, $t = 2/\pi$, $N = 99$, $\delta t = 0.16 \times 10^{-4}$. The filter parameters are $p = 50$ and $\theta = 0.3$

Table I. Note that, for this example a collocation method without viscosity (using the same discretisation parameters) fails.

We conclude that the *oscillatory numerical solution u^N contains high order information about the exact solution u.* This fact is proven for linear hyperbolic problems in [1] and seems to be valid for nonlinear problems. It is an interesting challenge to prove this.

2. *Stability.* To check the stability of the method we take the initial data:

$$u(x,0) = \begin{cases} 1, & \text{if } -1 \le x < 0, \\ -1, & \text{if } \quad 0 < x \le 1, \end{cases} \tag{4.5}$$

augmented with boundary conditions at ± 1. We take $u(-1, t) = 1$ and $u(+1, t) = -1$ for which the solution is a stationnary shock. We run the program for a long period and compare the solution obtained u^N ($N = 79$) with the initial data, $u^N(x, 0) = \mathcal{I}_N u(x, 0)$, the error in L^2-norm is plotted in Fig. 10.

3. *Expansion shock.* Riemann problem having an expansion shock. We take the initial data

$$u(x,0) = \begin{cases} -2, & \text{if } -1 \le x < 0, \\ 2, & \text{if } \quad 0 < x \le 1. \end{cases} \tag{4.6}$$

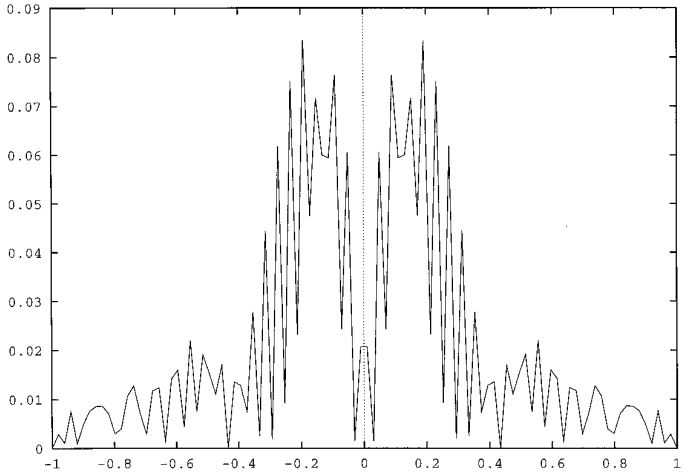

FIG. 10. Burgers equation, stability; differences $|u^N(x, t) - u^N(x, 0)|$ at time $t = 2$ for $N = 79$, $\delta t = 4\ 10^{-4}$.

The solution of this problem is an expansion shock. Let us recall that the basic finite difference centered schemes let the initial expansion be unchanged. For this problem the points ± 1 are outflow boundaries; at these points we use

$$\partial_t u^N(-1,t) + \partial_x \mathcal{I}_N f(u^N)(-1,t) = \varepsilon_N \partial_x \mathcal{Q}_m(\partial_x u^N)(-1,t) + \frac{\varepsilon_N}{\omega_N} \mathcal{Q}_m(\partial_x u^N)(-1,t)$$

$$\partial_t u^N(+1,t) + \partial_x \mathcal{I}_N f(u^N)(+1,t) = \varepsilon_N \partial_x \mathcal{Q}_m(\partial_x u^N)(+1,t) - \frac{\varepsilon_N}{\omega_N} \mathcal{Q}_m(\partial_x u^N)(+1,t).$$

Note that for $t > \frac{1}{2}$, the initial discontinuity leaves the computational domain, hence the solution becomes regular on the whole interval $[-1, 1]$. Figure 11 shows the (non filtered) solution at times $t = 1$, $t = 2$, and $t = 3$ for $N = 49$.

4.3. *Example* iii. *Nonconvex Flux*

The last scalar one-dimensional test is related to a nonconvex flux. Consider Eq. (1.1) with $f(u) = (u^2 - 1)(u^2 - 4)/4$ and the initial data:

$$u(x,0) = \begin{cases} -3, & \text{if } -1 \le x < 0, \\ 3, & \text{if } \quad 0 < x \le 1. \end{cases} \tag{4.7}$$

We solve this problem associated with outflow boundary conditions, the solution at time $t = 0.04$ ($N = 79$, $\delta t = 10^{-5}$) is plotted in Fig. 12 (the filter parameters are $p = 79$ and $\theta = 0.3$).

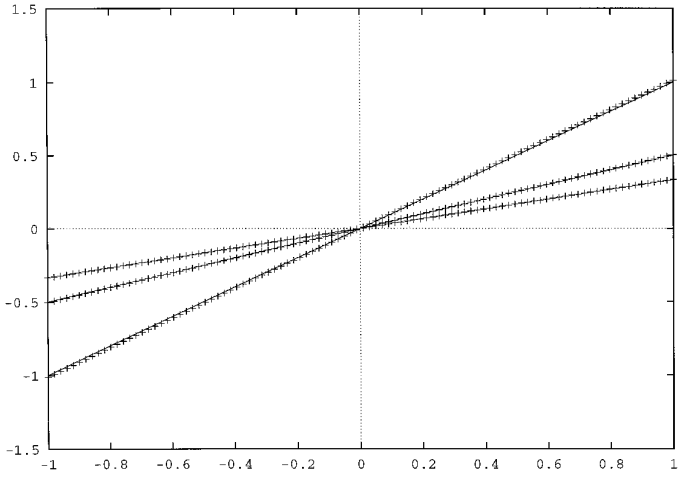

FIG. 11. Burgers equation, expansion shock; solution at times $t = 1$, $t = 2$, and $t = 3$ for $N = 49$, $\delta t = 10^{-4}$.

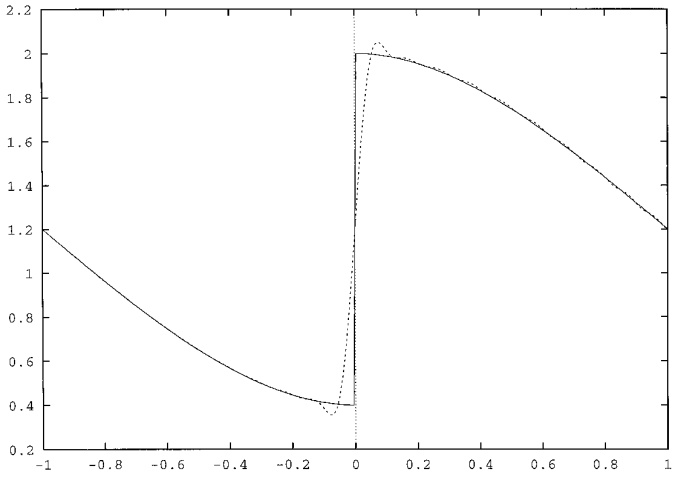

FIG. 13. 1D Euler system; the contact discontinuity problem (density), exact solution (solid line) and numerical solution (dashed line) at time $t = 2$, for $N = 80$, $\delta t = 10^{-4}$ and filter parameters $p = 40$, $\theta = 0.3$.

4.4. *Examples* iv. *Euler System of Gas Dynamics* (*1D*)

The Euler system of gas dynamics in conservative form is

$$\partial_t \mathbf{u} + \partial_x \mathbf{f}(\mathbf{u}) = 0 \tag{4.8}$$

where

$$\mathbf{u} = (\rho, \rho u, e)^{\mathrm{T}} \tag{4.9}$$

and

$$\mathbf{f}(\mathbf{u}) = (\rho u, p + \rho u^2, u(e + p))^{\mathrm{T}} \tag{4.10}$$

with the usual notation. ρ is the density of the fluid, u is the velocity, p is the pressure. The gas is assumed to be perfect and polytropic, $p = A(s)\,\rho^{\gamma}$, s is the entropy, e is the internal energy per volume unit: $e = \rho \mathrm{E} + \frac{1}{2}\rho u^2$ and E is the energy per mass unit: $(\gamma - 1)\mathrm{E} = p/\rho$. Equations (4.8) express respectively the laws conservation of mass, momentum and total energy for the fluid.

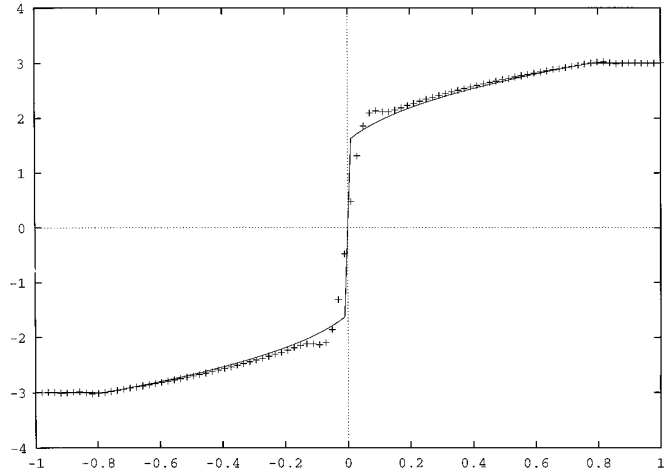

FIG. 12. Scalar equation with non convex flux and initial condition (4.7) solution at time $t = 0.04$ for $N = 79$, $\delta t = 10^{-5}$, $p = 79$, and $\theta = 0.3$.

1. *Contact discontinuity.* Consider the Euler system (4.8) with initial conditions $u = 1$, $p = 2$, and

$$\rho(x) = \begin{cases} \varphi(x-1), & \text{if } x < 0, \\ \varphi(x+1), & \text{if } x > 0, \end{cases}$$

where φ is a Hermit cubic that interpolates $\rho = 2$ and $\rho = 0.4$ with zero slope on each end of the interval $[-1, 1]$, φ is displaced so that the discontinuity is in the center of the domain. With these choices the flow is subsonic and the contact discontinuity moves through the domain; the original density profile translates with velocity u (see [7]). In the computations, we impose the exact solution at the boundary $x = -1$; the solution (density) for $N = 80$ and $\delta t = 10^{-4}$ is shown in Fig. 13 (the filter parameters are $p = 40$ and $\theta = 0.3$).

2. *The Sod shock tube problem.* Consider the Euler system (4.8) with initial conditions

$$\left.\begin{array}{l} \rho = 1 \\ u = 0 \\ p = 1 \end{array}\right\} \quad \text{for } x < x_0, \quad \left.\begin{array}{l} \rho = 0.125 \\ u = 0 \\ p = 0.1 \end{array}\right\} \quad \text{for } x > x_0.$$

We take $x_0 = 0$ and fix the exact solution at ± 1. In the computations, we use a scalar viscosity matrix; i.e., in (3.6) we take

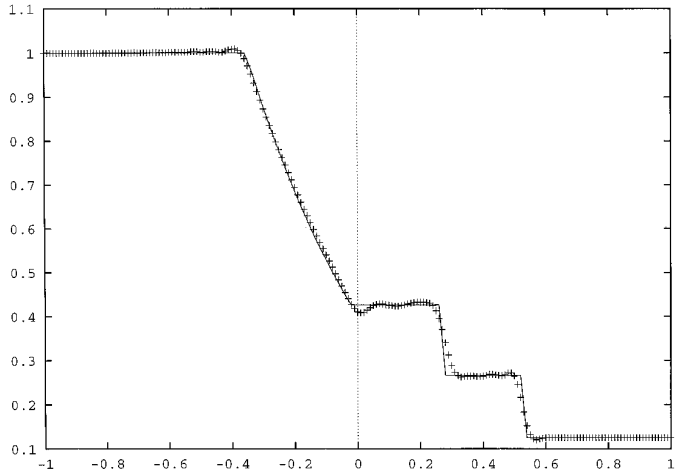

FIG. 14. 1D Euler system; the Sod shock tube problem, density at time $t = 0.3$, for $N = 149$, $\delta t = 0.15\ 10^{-4}$ and filter parameters $p = 60$, $\theta = 0.2$.

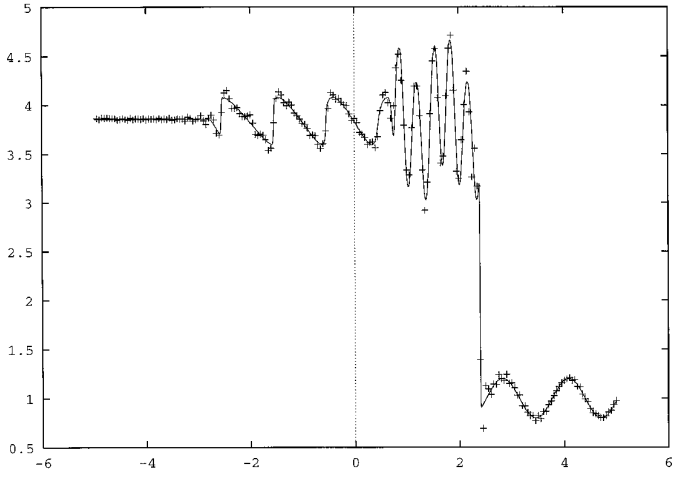

FIG. 15. 1D Euler system; the shock-disturbance problem, density at time $t = 0.36$, for $N = 199$, $\delta t = 10^{-5}$.

$$\varepsilon_1 = \varepsilon_2 = \varepsilon_3 = 1/N, \quad m_1 = m_2 = m_3 = 5\sqrt{N}.$$

The solution (density) for $N = 149$ is displayed in Fig. 14 (the filter parameters are $p = 60$, $\theta = 0.2$).

In this last example, the use of a high order method is no longer appropriate to reproduce the piecewise linear solutions. In the following example, high order methods are necessary to handle the solution.

3. *Shock-disturbance interactions.* Consider the Euler system (4.8) with initial conditions

$$\left.\begin{array}{l}\rho = 3.857143\\ u = 2.629369\\ p = 10.33333\end{array}\right\} \text{ for } x < x_0, \quad \left.\begin{array}{l}\rho = 1 + \lambda \sin(5x)\\ u = 0\\ p = 1\end{array}\right\} \text{ for } x > x_0$$

with $x_0 = -4$. This is a Mach 3 shock (that corresponds to $\lambda = 0$) interacting with sine waves in density. The fine structures in the density make it necessary to use a high order method. The original domain $[-5, 5]$ is mapped on the reference domain $[-1, 1]$. For the computations we take $\lambda = 0.2$ and fix the initial condition on the boundaries at ± 1. The (nonfiltered) density profile at time $t = 0.36$ for 200 points and $\delta t = 10^{-5}$ is shown in Fig. 15. The complicated flow field is well resolved; compare this with the results presented in [15]. In this reference, it is shown that a second-order MUSCL-type TVD scheme with 800 points does not catch the fine details in the density solution. The "exact" solution (solid line) is the converged one obtained by a third-order ENO scheme with 1200 points (private communication of Prof. C. W. Shu).

Let us recall that the filtering procedure (3.9) involves two parameters θ and p. The filtered solution displayed in Fig. 16 corresponds to $p = 60$, $\theta = 0.2$; for this choice, the fine scales are destroyed while the large ones are quite well reproduced. This is typically what low resolution schemes do. In contrary, the choice $p = 100$, $\theta = 0.4$ (see Fig. 17) gives a good resolution of the fine scales but does not really improve the solution in the large scales.

4.5. *Examples* v. *Linear Equations* (*2D*)

These problems deal with 2D linear systems.

1. *Contact Discontinuity.* Recall that usually the finite difference numerical schemes smear more severely the contact discontinuities (linear discontinuities) than the shocks (nonlinear discontinuities). This test shows that the

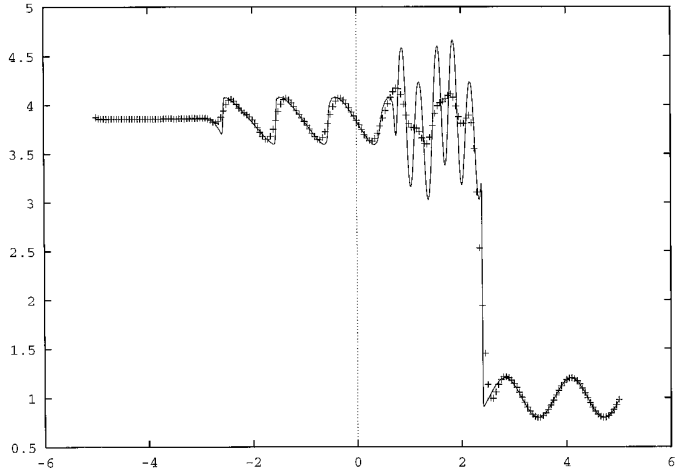

FIG. 16. 1D Euler system; the shock-disturbance problem, the same as before, filtered solution $p = 60$, $\theta = 0.2$.

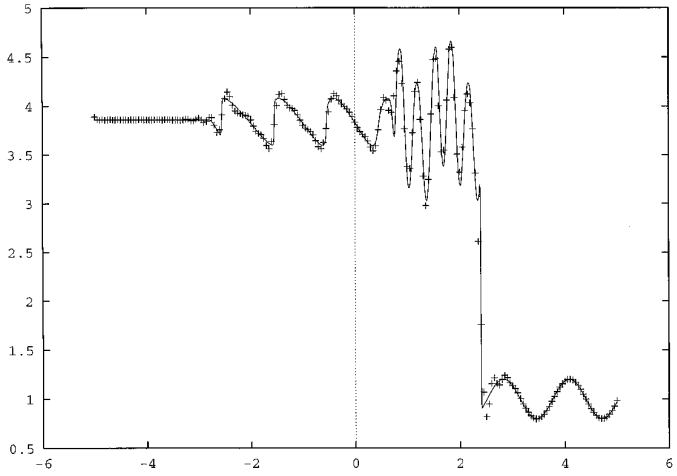

FIG. 17. 1D Euler system; the shock-disturbance problem, the same as before, filtered solution $p = 100$, $\theta = 0.4$.

spectral viscosity method gives a good resolution of multi-dimensional contact discontinuities. The problem is to find $u(x, y, t)$ such that

$$\partial_t u + \partial_x u + \partial_y u = 0 \tag{4.11}$$

with the initial discontinuous data:

$$u_0(x, y) = \begin{cases} 0.5, & \text{if } x^2 + y^2 \le R^2 \\ 0, & \text{if } x^2 + y^2 > R^2. \end{cases} \tag{4.12}$$

This discontinuity will propagate at a constant speed and height. This problem is well-posed if we impose boundary conditions on the sides $x = -1$ and $y = -1$. We take $u(-1, y, t) = \tilde{u}(-1, y, t)$ and $u(x, -1, t) = \tilde{u}(x, -1, t)$, where $\tilde{u}$ is the solution of the associated periodic problem, the exact solution is then $u \equiv \tilde{u}$. The Legendre viscosity approximation of this problem leads to find $u^{N,M}(x, y, t) \in \mathbb{P}_{N,M}$, the space of algebraic polynomials of two variables with degree in x (resp. y) less than or equal to N (resp. M) satisfying for all $\varphi \in \mathbb{P}_{N,M}$

$$\begin{aligned} &((\partial_t u^{N,M} + \partial_x \mathcal{I}_N f(u^{N,M}) \\ &\quad + \partial_y \mathcal{I}_M g(u^{N,M}), \varphi))_{N,M} \\ &= -\varepsilon_1((\mathcal{Q}_{m1} \partial_x u^{N,M}, \partial_x \varphi))_{N,M} \\ &\quad - \varepsilon_2((\mathcal{Q}_{m2} \partial_y u^{N,M}, \partial_y \varphi))_{N,M} \\ &\quad + ((\mathcal{B}(u^{N,M}), \varphi))_{N,M}, \end{aligned}$$

where $((\cdot, \cdot))_{N,M}$ denotes the 2D discrete scalar product related to the Gauss–Lobatto Legendre nodes:

$$\begin{aligned} ((f, g))_{N,M} &= \sum_{i=0}^{N} \sum_{j=0}^{M} f(\xi_i^N, \xi_j^M) g(\xi_i^N, \xi_j^M) w_i^N w_j^M \\ &\simeq \int_{-1}^{1} \int_{-1}^{1} f(x, y) g(x, y)\, dx\, dy. \end{aligned}$$

Choosing $\varphi = h_{i,j} = h_i(x) h_j(y)$, one obtains

- at inner points ($1 \le i \le N - 1$ and $1 \le j \le M - 1$):

$$\begin{aligned} &\partial_t u^{N,M}(\xi_i, \xi_j, t) + \partial_x \mathcal{I}_N f(u^{N,M})(\xi_i, \xi_j, t) \\ &\quad + \partial_y \mathcal{I}_M g(u^{N,M})(\xi_i, \xi_j, t) \\ &= \varepsilon_1 \partial_x \mathcal{Q}_{m1} \partial_x u^{N,M}(\xi_i, \xi_j, t) \\ &\quad + \varepsilon_2 \partial_y \mathcal{Q}_{m2} \partial_y u^{N,M}(\xi_i, \xi_j, t) \end{aligned}$$

- on the right boundary $x = 1$, $y \ne -1$, and $y \ne 1$:

$$\begin{aligned} &\partial_t u^{N,M}(1, \xi_j, t) + \partial_x \mathcal{I}_N f(u^{N,M})(1, \xi_j, t) \\ &\quad + \partial_y \mathcal{I}_M g(u^{N,M})(1, \xi_j, t) \\ &= \varepsilon_1 \partial_x \mathcal{Q}_{m1} \partial_x u^{N,M}(1, \xi_j, t) \\ &\quad + \varepsilon_2 \partial_y \mathcal{Q}_{m2} \partial_y u^{N,M}(1, \xi_j, t) \\ &\quad - (\varepsilon_1 / w_N)\, \mathcal{Q}_{m1} \partial_x u^{N,M}(1, \xi_j, t) \end{aligned}$$

- on the bottom boundary $y = 1$, $x \ne -1$, and $x \ne 1$:

$$\begin{aligned} &\partial_t u^{N,M}(\xi_i, 1, t) + \partial_x \mathcal{I}_N f(u^{N,M})(\xi_i, 1, t) \\ &\quad + \partial_y \mathcal{I}_M g(u^{N,M})(\xi_i, 1, t) \\ &= \varepsilon_1 \partial_x \mathcal{Q}_{m1} \partial_x u^{N,M}(\xi_i, 1, t) \\ &\quad + \varepsilon_2 \partial_y \mathcal{Q}_{m2} \partial_y u^{N,M}(\xi_i, 1, t) \\ &\quad - (\varepsilon_2 / w_M)\, \mathcal{Q}_{m2} \partial_y u^{N,M}(\xi_i, 1, t) \end{aligned}$$

- at the corner $x = 1$, $y = 1$:

$$\begin{aligned} &\partial_t u^{N,M}(1, 1, t) + \partial_x \mathcal{I}_N f(u^{N,M})(1, 1, t) \\ &\quad + \partial_y \mathcal{I}_M g(u^{N,M})(1, 1, t) \\ &= \varepsilon_1 \partial_x \mathcal{Q}_{m1} \partial_x u^{N,M}(1, 1, t) \\ &\quad + \varepsilon_2 \partial_y \mathcal{Q}_{m2} \partial_y u^{N,M}(1, 1, t) \\ &\quad - (\varepsilon_1 / w_N)\, \mathcal{Q}_{m1} \partial_x u^{N,M}(1, 1, t) \\ &\quad - (\varepsilon_2 / w_M)\, \mathcal{Q}_{m2} \partial_y u^{N,M}(1, 1, t). \end{aligned}$$

The solution at time $t = 2$ (one period) is displayed in

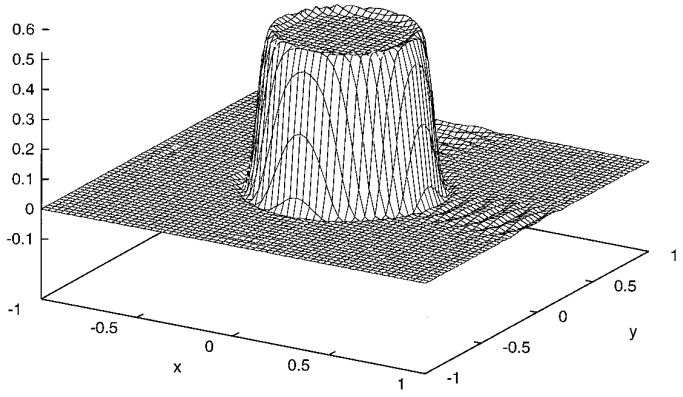

FIG. 18. The 2D linear advection equation; solution ($N = M = 80$) at time $t = 2$.

Fig. 18. The parameters of the calculations are $R = 0.4$, $N = 80$ in each direction, $\delta t = 510^{-5}$; the parameters of the filtering procedure are $p = 40$, $\theta = 0.3$ in each direction. The solution is now quite well reproduced.

2. *Nondissipation.* Although centered, the spectral methods are not dissipative. Consider the rotating hill problem,

$$\partial_t u - y\partial_x u + x\partial_y u = 0, \tag{4.13}$$

and the initial data,

$$u_0(x, y) = \begin{cases} 1 - R(x, y)/R_0, & \text{if } R(x, y) \le R_0 \\ 0, & \text{if } R(x, y) \le R_0 \end{cases} \tag{4.14}$$

with $R(x, y) = ((x - x_c)^2 + (y - y_c)^2)^{1/2}$. The exact solution of this problem is $u(x, y, t) = u_0(X, T)$, where (X, Y) are obtained from (x, y) by a rotation of angle t,

$$\begin{pmatrix} X \\ Y \end{pmatrix} = \begin{pmatrix} \cos t \sin t \\ -\sin t \cos t \end{pmatrix} \begin{pmatrix} x \\ y \end{pmatrix}.$$

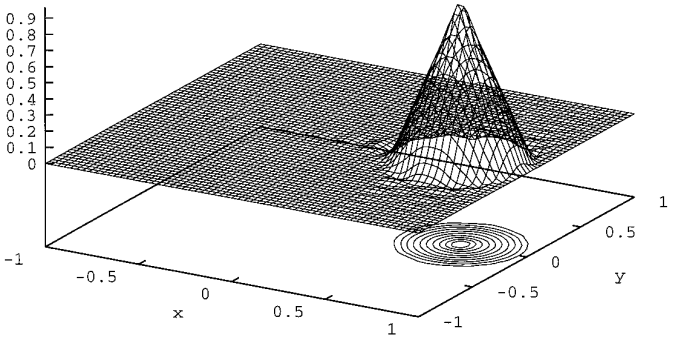

FIG. 19. The rotating hill; initial data ($N = M = 40$).

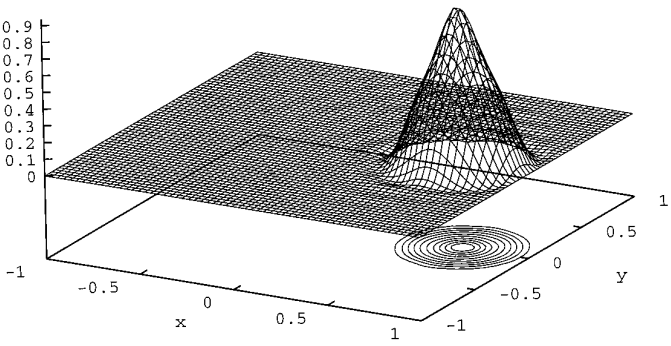

FIG. 20. The rotating hill; solution at time $t = 6.2832$, for $N = M = 40$, $\delta t = 3.1415/1000$.

The cone, centered at (x_c, y_c) rotates around the origin with periodicity $T = 2\pi$. In the computations, we take $(x_c, y_c) = (0.65, 0)$ and $R_0 = \frac{1}{3}$, $N = M = 40$, $\delta t = 10^{-3}\pi$. The initial cone is plotted in Fig. 19; the maximum height of $u_0(x, y)$ on the grid is $\simeq 0.96$. The nonfiltered numerical solution after a revolution is displayed in Fig. 20; the maximum height is $\simeq 0.9$. For more precise comparison, we plot in Fig. 21 the sections $y = 0$ of the initial data and the solution at time 2π. The peak is quite well reproduced. Note that the viscosity parameters are the same as those used in the computation of the discontinuous solution of the preceding test. We conclude that the viscosity needed to compute a discontinuous solution does not deteriorate the approximation of a more regular solution.

4.6. *Examples* vi. *Euler System of Gas Dynamics* (*2D*)

The two dimensional Euler's equations of gas dynamics are

$$\partial_t \mathbf{u} + \partial_x \mathbf{f}(\mathbf{u}) + \partial_y \mathbf{g}(\mathbf{u}) = 0 \tag{4.15}$$

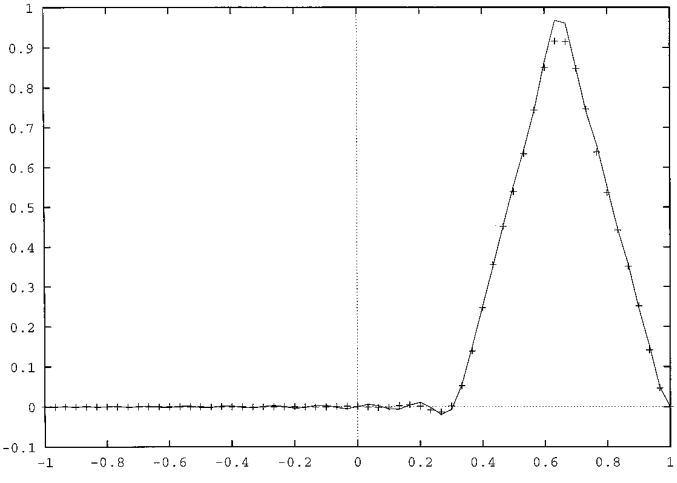

FIG. 21. The rotating hill; sections $y = 0$ of the initial data (solid line) and the solution (+) at time $t = 6.2832$.

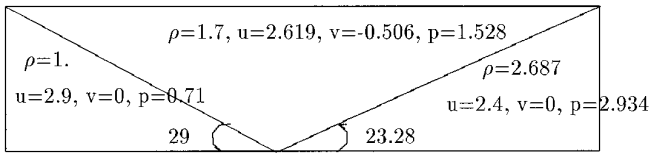

FIG. 22. Exact solution of the shock reflection problem.

$$\mathbf{u}(x, y, 0) = \mathbf{u}_0(x, y) \tag{4.16}$$

with $\mathbf{u} = (\rho, \rho u, \rho v, e)$. The fluxes $\mathbf{f}$ and $\mathbf{g}$ are defined by

$$\mathbf{f} = (\rho u, p + \rho u^2, \rho uv, (e + p)u) \tag{4.17}$$

$$\mathbf{g} = (\rho v, \rho uv, p + \rho v^2, (e + p)v). \tag{4.18}$$

ρ is the fluid density, u and v are respectively the components of the velocity, p is the pressure. The gas is assumed to be perfect and polytropic, $p = (\gamma - 1)(e - \frac{1}{2}\rho(u^2 + v^2))$, $\gamma = 1.4$ and e is the energy per volume unit, $e = \rho \mathrm{E} + \frac{1}{2}\rho(u^2 + v^2)$, where E is the internal energy per unit mass: $(\gamma - 1)\mathrm{E} = p/\rho$.

1. *Reflection of a shock* (consult [6]). We study the reflection of an oblique shock on the lower side of a rectangular domain defined by $0 \le \xi \le 4.12829$, $0 \le \eta \le 1$. The initial flow is given by

$$\rho = 1, \quad u = 2.9, \quad v = 0, \quad p = 1/1.4.$$

The boundary conditions are:

• inflow boundary conditions on $\xi = 0$, where all the variables are fixed taking the same values as at initial time;

• outflow boundary conditions on the side $\xi = 4.12829$, where no variable is imposed.

• reflection condition on the lower side $\eta = 0$,

$$v(\xi, 0) = 0;$$

• fixed values on the upper side $\eta = 1$ (those of the exact solution):

$$\rho = 1.7, \quad u = 2.61932, \quad v = -0.506339, \quad p = 1.52824.$$

The exact solution is formed by an incident shock with angle 29° and a reflected shock with angle 23.28°; see Fig. 22. The solution after the second shock is

$$\rho = 2.68732, \quad u = 2.40148, \quad v = 0, \quad p = 2.93413.$$

The physical domain is mapped on the unit square $[-1, 1] \times [-1, 1]$, the discretisation parameters are $N_x = N_y = N = 80$, $m = 2\sqrt{N}$, $\delta t = 2.5 \times 10^{-5}$. The reflection conditions are imposed (on the conservative variables) by simple linear interpolation: $\rho(\xi_i, \xi_0) = \rho(\xi_i, \xi_1), p(\xi_i, \xi_0) = p(\xi_i, \xi_1), u(\xi_i, \xi_0) = -u(\xi_i, \xi_1), v(\xi_i, \xi_0) = 0$. The solution (pressure) after the shock leaves the domain is plotted in Fig. 22 and the numerical solution is displayed Figs. 23 and 24; the filter parameters are $\theta = 0.3, p = 50$ in each direction.

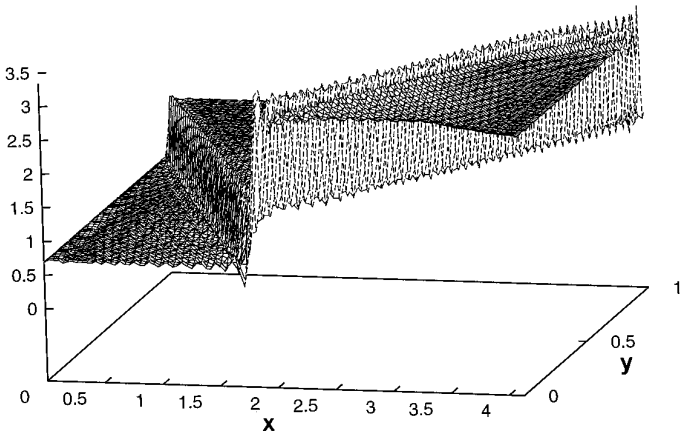

FIG. 23. The shock reflection problem. Solution (pressure) for $N = 80$, $M = 80$.

2. *Interaction between a shock wave and a rotating vortex* [4]. In this example, we consider the interaction between a Mach 3 shock wave moving from the left to the right and a rotating vortex initially located to the right side of the shock. The shock front will be deformed by the vortex and pressure waves are generated; consult [4] for details. The velocity field of the vortex is the one induced by two rotating concentric cylinders with radius r_1 and r_2, respectively ($r_1 < r_2$). Initially the vortex is located at the point (x_c, y_c). The outsider cylinder is stationary and the

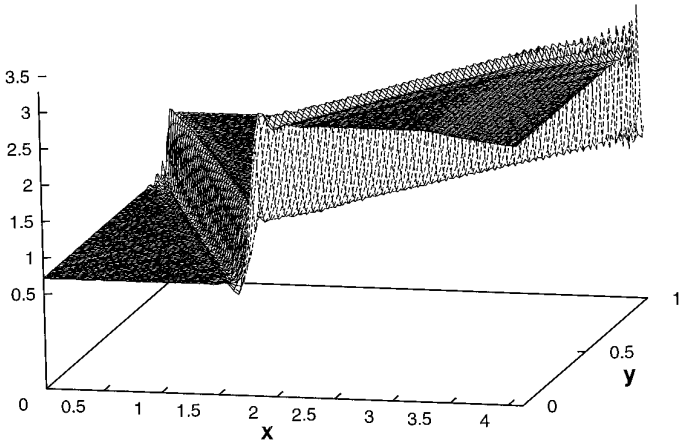

FIG. 24. The shock reflection problem. Filtered solution, $p = 50$, $\theta = 0.3$.

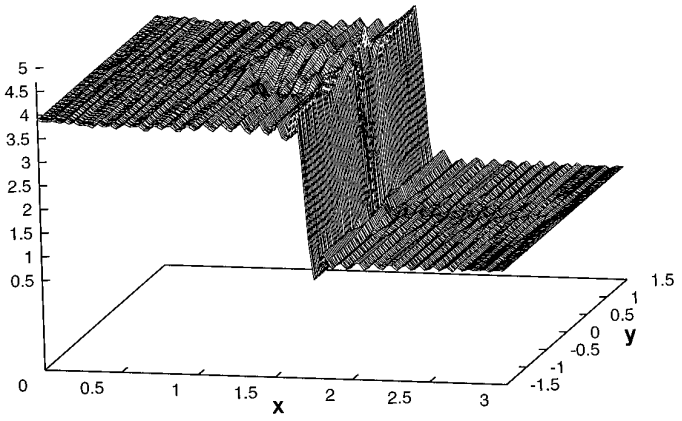

FIG. 25. Shock-vortex interaction. Density at time $t = 0.4$ ($N_x = 80$, $N_y = 80$).

inside one rotates with the angular velocity w. Let $\tilde{v}(r)$ be the radius velocity at a distance r from the center of the vortex; we have:

$$v(r) = \begin{cases} wr, & \text{if } 0 \le r \le r_1, \\ w\left(\dfrac{1}{ra} + \dfrac{rr_1^2}{b}\right), & \text{if } r_1 \le r \le r_2, \\ 0, & \text{if } r \ge r_2, \end{cases}$$

where $a = r_1^{-2} - r_2^{-2}$, $b = r_1^2 - r_2^2$, and $r = ((x - x_c)^2 + (y - y_c)^2)^{1/2}$. The velocity (u, v) induced by this vortex is

$$\tilde{v}_x(r) = -\frac{y - y_c}{r} v(r)$$

$$\tilde{v}_y(r) = \frac{x - x_c}{r} v(r),$$

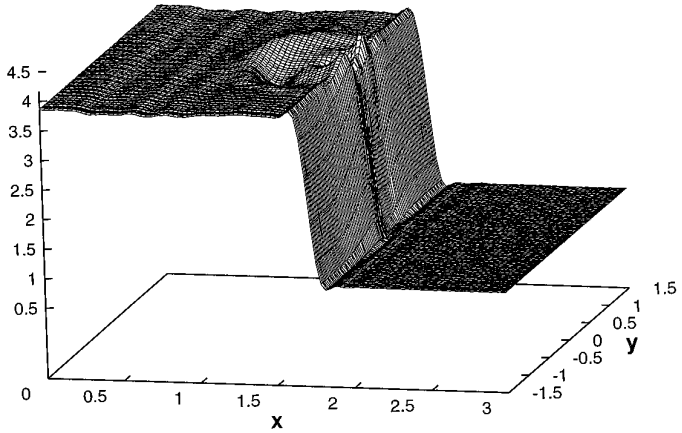

FIG. 26. Shock-vortex interaction. The same as before, filtered in the x-direction ($p = 40$, $\theta = 0.3$).

where $(x_c, y_c) = (1.05, 0)$. The initial conditions for the simulation are

$$\left.\begin{array}{l} \rho_L = 3.857143 \\ u_L = 2.629367 \\ v_L = 0 \\ p_L = 10.333333 \end{array}\right\} \quad \text{if } x < x_0, \qquad \left.\begin{array}{l} \rho_R = 1 \\ u_R = \tilde{v}_x(r) \\ v_R = \tilde{v}_y(r) \\ p_R = 1 \end{array}\right\} \quad \text{if } x > x_0,$$

where x_0 is the initial shock position. In the computations, we take $r_1 = 0.15$, $r_2 = 0.75$, $w = 7.5$, and $x_0 = 0.3$.

The boundary conditions are:

- left and right sides: we keep the same field as at initial time. This is valid as long as the waves do not reach these boundaries.
- bottom and top sides: we assign values computed by the spectral scheme.

Here again the physical domain $[0, 3] \times [-1.5, 1.5]$ is mapped on the unit square $[-1, 1] \times [-1, 1]$; the discretisation parameters are $N_x = 80$, $N_y = 80$, $m_x = 2\sqrt{N_x}$, $m_y = 2\sqrt{N_y}$, $\delta t = 10^{-4}$. The viscosity solution (density) at time $t = 0.4$ is displayed in Fig. 25. This solution is filtered in the x-direction (parameters $p = 40$, $\theta = 0.3$); see Fig. 26.

5. CONCLUSION

A new spectral shock-capturing method, the Legendre spectral vanishing viscosity (LSVV) method was implemented to solve nonlinear conservation laws. This method consists in applying a ''spectral'' viscosity on the high wavenumbers of the numerical solution. This viscosity is just strong enough to stabilize the calculations, but sufficiently small to retain the spectral accuracy. The results obtained especially for the Euler system of gas dynamics are very stimulating. The numerical solution when filtered gives a good approximation of the exact entropic solution. However, near the discontinuity the filter procedure does not work well. The use of the new filters analysed in [9] will improve the results; indeed such filters are efficient even at the discontinuity location.

Some difficulties are not considered in this paper, namely complicated boundary conditions and complex geometries. These points are currently under investigations in [8] by a multidomain approach.

ACKNOWLEDGMENTS

The 2D Euler tests were performed on the CRAY C98 of the Institut du Développement et des Ressources en Informatique Scientifique; the author thanks this authority for its support.

REFERENCES

1. S. Abarbanel, D. Gottlieb, and E. Tadmor, "Spectral Methods for Discontinuous Problems," in *Numerical Methods for Fluid Dynamics II*, edited by K. W. Morton and M. J. Baines (Oxford Univ. Press, Oxford, 1986).
2. O. Andreassen, I. Lie, and C. E. Wasberg, *J. Comput. Phys.* **94**(2) (1989).
3. C. Bernardi and Y. Maday, *Approximations spectrales de problèmes elliptiques* (Springer-Verlag, New York/Berlin, 1992).
4. W. Cai and C. W. Shu, *J. Comput. Phys.* **104,** 427 (1993).
5. C. Canuto, M. Y. Hussaini, A. Quarteroni, and T. A. Zang, *Spectral Methods in Fluid Dynamics* (Springer-Verlag, New York/Berlin, 1988).
6. B. Cockburn and C. W. Shu, Technical Report 32, ICASE, 1991 (unpublished).
7. S. F. Davis, *Appl. Numer. Math.* **10,** 447 (1992).
8. L. Emmel, Ph.D. thesis, Université Pierre et Marie Curie, in preparation.
9. D. Gottlieb, C. W. Shu, A. Solomonoff, and H. Vandeven, *J. Comput. Appl. Math.* **43** (1992).
10. D. Gottlieb and E. Tadmor, *Math. Comput.* **56,** 565 (1991).
11. F. Lafon and S. Osher, *J. Comput. Phys.* **96,** 111 (1992).
12. P. D. Lax, *Hyperbolic Systems of Conservation Laws and the Mathematical Theory* of Shock Waves, CBMS-NSF Regional Conference Series in Applied Mathematics, Vol. 11 (SIAM, Philadelphia, 1972).
13. Y. Maday and E. Tadmor, *SIAM J. Numer. Anal.* **26**(4) (1989).
14. Y. Maday, S. M. Ould Kaber, and E. Tadmor, *SIAM J. Numer. Anal.* **30**(2) (1993).
15. C. W. Shu and S. Osher, *J. Comput. Phys.* **83**(1) (1989).
16. S. M. Ould Kaber, Ph.D. thesis, Université Pierre et Marie Curie, 1991 (unpublished).
17. S. M. Ould Kaber, *Comput. Methods Appl. Mech. Engrg.* **116,** 123 (1994).
18. S. Schochet, *SIAM J. Numer. Anal.* **27,** 1142 (1990).
19. E. Tadmor, *SIAM J. Numer. Anal.* **26**(1) (1989).
20. E. Tadmor, *Comput. Methods Appl. Mech. Engrg.* **80,** 197 (1990).